# EEM-PARAFAC as a convenient methodology to study fluorescent emerging pollutants degradation: (fluoro)quinolones oxidation in different water matrices

Iván Sciscenko [a,*], Margarita Mora [b], Pau Micó [c], Carlos Escudero-Oñate [d], Isabel Oller [e,f], Antonio Arques [a]

[a] Departamento de Ingeniería Textil y Papelera, Universitat Politècnica de València (UPV), Plaza Ferrándiz y Carbonell S/N, 03801 Alcoy, Spain
[b] Departamento de Matemática Aplicada, Universitat Politècnica de València, Plaza Ferrándiz y Carbonell S/N, 03801 Alcoy, Spain
[c] Departamento de Informática de Sistemas y Computadores, Universitat Politècnica de València, Plaza Ferrándiz y Carbonell S/N, 03801 Alcoy, Spain
[d] Institute for Energy Technology (IFE), Instituttveien 18, 2007 Kjeller, Norway
[e] CIEMAT-Plataforma Solar de Almería, Carretera de Senés km 4, 04200 Tabernas, Spain
[f] CIESOL, Joint Centre of the University of Almería-CIEMAT, Ctra. Sacramento s/n, 04120 Almería, Spain

## HIGHLIGHTS

- Solar-Photo-Fenton was employed to degrade (fluoro)quinolones mixtures.
- PARAFAC was able of deconvoluting the overlapping signals from every compound.
- By-products molecular structures can be tentatively predicted with EEM-PARAFAC.
- Interaction fluoroquinolone-iron enhanced the removal of thiabendazole.

## GRAPHICAL ABSTRACT
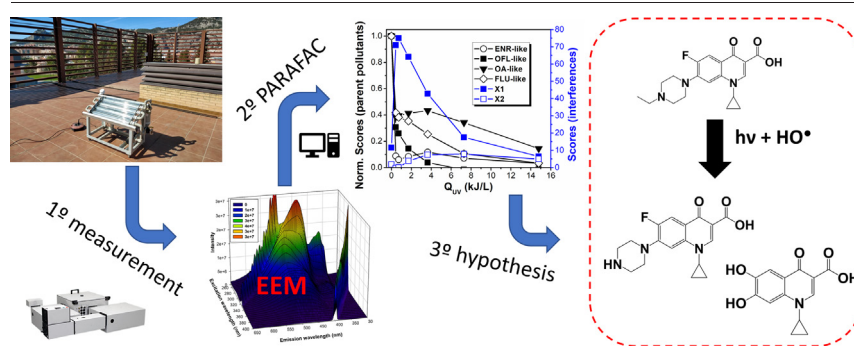


## ARTICLE INFO

## ABSTRACT

Commercial (fluoro)quinolones ((F)Qs), ciprofloxacin (CIP), enrofloxacin (ENR), ofloxacin (OFL), oxolinic acid (OA) and flumequine (FLU) (3 μM each), were degraded with solar-photo-Fenton in a compound parabolic concentrator photoreactor (total volume 5 L) in ultra-pure water at pH = 5.0, salty water at pH = 5.0, and simulated wastewater at pH = 5.0 and 7.5. Iron speciation (its hydrolysis and the complexation with (F)Qs 15 μM and/or chlorides 0.5 M) was calculated at pH 5.0, observing, negligible formation of Fe(III)-chloride complexes, and that >99 % of the total (F)Qs are forming complexes stoichiometry 1:1 with Fe(III) (which also increases the percentage of Fe $(OH)^{2+}$), being minoritarian the free antibiotic form. On the other hand, EEM-PARAFAC (fluorescence excitation-emission matrices-parallel factor analysis) was employed to simultaneously study the behaviour of: i) 4 structure-related groups corresponding to parent pollutants and slightly oxidised by-products, ENR-like (including CIP), OFL-like, OA-like, FLU-like; ii) intermediates still showing (F)Q characteristics (exhibiting analogous fluorescent fingerprint to ENR-like one, but shifted to shorter wavelengths); iii) humic-like substances. The scores from the 4 PARAFAC components corresponding to the parent pollutants were plotted vs. accumulated energy, exhibiting slower decay than their individual removals (measured with HPLC-UV/vis) due to the contribution of the aforementioned by-

products to the overall fluorescence. Moreover, thiabendazole (TBZ) 3 μM was added as fluorescence interference. The presence of (F)Qs greatly enhanced TBZ degradation due to (F)Q-Fe(III) complex formation, keeping iron active at pH = 5.0 for Fenton process. The EEM-PARAFAC model was able to recognise the former six components plus an additional one attributable to TBZ-like.

## 1. Introduction

Antibiotics are the pharmaceuticals with the highest detection frequency and concentration in receiving waters of the world, especially quinolones and fluoroquinolones (together denoted as (F)Qs from now on) (Feng et al., 2018; Gou et al., 2021; Van Doorslaer et al., 2014). In fact, a median global concentration of 164 μg/L has been reported for the FQ, ciprofloxacin, in freshwater ecosystems. This is a concentration 2 to 4 orders of magnitude higher than most pharmaceuticals, which is explained mainly due to the large discharges from Asiatic countries, predominantly China and India (Hughes et al., 2013). The main concern of these substances is the likelihood of developing antibiotic-resistant genes and bacteria, which can seriously threaten societies (Delalay et al., 2020; Oliveira et al., 2020). Particularly in wastewater treatment plants, two characteristics make them a perfect environment for the development of antibiotic resistances: i) the large bacterial concentration in these effluents per day and per inhabitant equivalent ($10^9$–$10^{12}$ Colony Forming Units), and ii) the exposure of the bacterial communities to sub-inhibitory concentrations of antibiotics. Therefore, it is estimated that approximately 1 % of total Colony Forming Units will certainly exhibit antibiotic resistance (Rizzo et al., 2013).

Toward wastewater reclamation, research to address antibiotic environmental impact and the development of their remediation strategies (as well as for other so-called contaminants of emerging concern, CECs) has received increasing attention in the last years. Advanced Oxidation Processes (AOPs) —where highly reactive species, such as hydroxyl radical (HO•), are generated— arise as a more efficient option compared to the classical use of chlorine or ozone. AOPs can deal with bio-recalcitrant organic pollutants and bacterial content and avoid the formation of carcinogenic disinfection by-products (Nikolaou and Lekkas, 2001; Oturan and Aaron, 2014). Fenton reaction is a widely known AOP, which is enhanced by the action of light and is defined as solar-photo-Fenton when using sunlight (Carra et al., 2014). Different research groups have studied the application of dark-Fenton and photo-Fenton in the last decade (Bokare and Choi, 2014; Lin et al., 2022; Pignatello et al., 2006).

Although several articles are studying the degradation of a specific type of contaminant (such as fluoroquinolones) with, i.e., different photocatalysts, AOPs or reactors, most of them only focus on the degradation of the parent pollutant, and not in the formed by-products, and, if they do so, they employ mass spectrometry, which is expensive and not frequent within research groups. To overcome this problem, the development of methods based on accessible equipment, able to track the pollutants abatement simultaneously (i.e. without a previous separation method) and in a non-time consuming way, are necessary. In this context, fluorescence excitation-emission matrices-parallel factor analysis (EEM-PARAFAC) can be employed. This tool is commonly used for dissolved organic matter (DOM) characterization and monitoring among wastewater or drinking water treatment plants (Cui et al., 2022; Shutova et al., 2014; Xu et al., 2021; Yang et al., 2015).

Basically, a EEM is a three-dimensional plot of fluorescence intensity, and excitation and emission wavelengths, obtaining a topographic surface resulting from the different fluorophores present in the sample. Therefore, each individual fluorophore might have a characteristic fingerprint which might overlap with the analogous of another compound. In these cases, mathematical tools, such as PARAFAC, can be employed to deconvolute the overlapped signals within a EEM into its individual components, thus unveiling the contribution of each fluorophore (Murphy et al., 2013). When several species have highly similar fingerprints, they are not

deconvoluted by the algorithm, being identified as just one component. This is not necessarily a drawback, as EEM-PARAFAC allows the classification of the compounds in families, without needing to identify every single component, an issue becoming particularly relevant when monitoring pollutants treatment, as a high number of by-products, with slight structural differences, might be formed.

Some efforts have been recently devoted to extending the use of EEM-PARAFAC to follow the degradation/adsorption of CECs (Carabajal et al., 2017; Sgroi et al., 2017). In this regard, two recent papers have been reported applying EEM-PARAFAC to study FQs oxidative transformation (Sciscenko et al., 2021b, 2020); in these works, the EEM were measured in time-course experiments and processed with PARAFAC, demonstrating to be a suitable methodology to track: i) the FQs degradation, ii) the generated by-products formation and elimination kinetics, and iii) major molecular structural modifications when comparing photolysis against (photo-)Fenton processes. Most importantly, a good correlation between PARAFAC component scores (fluorescence intensity) and antibiotic activity decay was observed, indicating that this methodology could be a fast approach to estimate when the fluorescent CECs reactive site —the environmentally relevant moiety to eliminate— is oxidised. However, the aforementioned published works are still far away from demonstrating the real applicability of this procedure since the studied systems were relatively simple: high pollutant concentrations (10–25 mg/L), acidic conditions (pH = 3, optimal for Fenton-based processes, but far away from real wastewater effluents), absence of other water constituents (e.g. DOM, carbonates or phosphates) and with experiments carried out at laboratory scale using lamps as irradiation source.

As a logical step forward, in this work we employed a more complex system to test the aforementioned methodology, using a mixture of a higher number of contaminants, at concentrations closer to that of real effluents, dissolved in different water matrices also containing fluorescence interferences (e.g. DOM and other fluorescent CEC) and performing the experiments at pilot plant scale with real sunlight. Accordingly, a mixture of 5 (F)Q-antibiotics, ofloxacin (OFL), ciprofloxacin (CIP), enrofloxacin (ENR), oxolinic acid (OA) and flumequine (FLU), was employed; these compounds have been chosen as they are typically found in wastewater treatment plant effluents (Ezzariai et al., 2018; Ormeno-Cano and Radjenovic, 2022; Van Doorslaer et al., 2014) and their EEM fingerprints are expected to be similar, thus, challenging to deconvolute. In addition, different water matrices were tested: ultra-pure water (MQ), simulated wastewater (SWW) and salty water (SW). In particular, the latter is relevant to studying the effect of high concentration of chlorides (>1 g/L), present in wastewater effluents with industrial inputs (Grebel et al., 2010), retentates from nanofiltration systems (Salmerón et al., 2021) or ballast water (Moreno-Andrés et al., 2019); we employed 30 g/L of NaCl as SW, mainly focused on seawater due to the high occurrence of (F)Qs in marine environments linked to direct discharge when used in fish farms (Lu et al., 2020; Rusu et al., 2015). Then an additional interference, thiabendazole (TBZ), was added to the system to test the ability of PARAFAC to detect and identify plausible strong non-calibrated substances. The studied process has been solar-photo-Fenton, scaled-up to pilot plant and with relatively low concentrations of pollutants.

## 2. Experimental

### 2.1. Reagents

Thiabendazole (TBZ), flumequine (FLU), oxolinic acid (OA), ofloxacin (OFL), enrofloxacin (ENR) and ciprofloxacin (CIP) (molecular structures

shown in Fig. 1) high purity (>99 %), gum Arabic, lignin sulphonic acid sodium, peptone, and humic acid substances were purchased from Sigma-Aldrich. Beef extract from Bovril. $FeSO_4 \cdot 7H_2O$, $H_2O_2$ (33 % *w/v*), $NaHCO_3$, NaCl, $(NH_4)_2SO_4$, NaOH, acetic acid (96 %), 1,10-phenanthroline 1-hydrate, $H_2SO_4$ (96 %), and UHPLC grade methanol and acetonitrile, were obtained from AppliChem-Panreac. Ammonium acetate, $K_2HPO_4$, $MgSO_4 \cdot 7H_2O$, $CaSO_4 \cdot 2H_2O$ and ascorbic acid were purchased from Scharlau, and formic acid (80 %) from VWR Chemicals. Ultra-pure water (MQ) was prepared with a Merck Milli-Q system. FLU, OA, OFL, ENR and CIP 300 µM stock solutions were prepared in basic media and TBZ 300 µM in acidic media. All the solutions were stable when preserved in the dark, and no hydrolysis was observed.

### 2.2. Degradation experiments

Degradation of the 5 (F)Qs mixture was performed with solar-photo-Fenton in a tubular pilot plant based on a CPC (Compound Parabolic Concentrator) reactor (Solardetox Acadus-2001) described in detail elsewhere (Malato et al., 2009; Soler et al., 2011). It consists of four borosilicate tubes with total irradiated area of 0.26 $m^2$, two aluminum parabolic surfaces to concentrate the sunlight in each tube axis, and supported in a platform tilted 30° with the horizon. The plant was always oriented to the South, and it was located in Alcoy (East of Spain). For each experiment, the plant was loaded with 5 L of solution containing 3 µM of each antibiotic which was constantly recirculated through the tubes. Accumulated energy ($Q_{UV}$) was used as variable to plot degradation kinetics, which is calculated by Eq. (1) (Prieto-Rodríguez et al., 2013):

$$Q_{UV,n} = Q_{UV,n-1} + \Delta t I_{UV} \frac{A_i}{V_T} \qquad (1)$$

where $\Delta t$ (s) is the experimental time, $I_{UV}$ (W/m$^2$) the ultraviolet radiation (measured with a radiometer, Acadus 85, placed on top of the pilot plant), $A_i$ (m$^2$) the irradiated surface and $V_T$ (L) the total volume.
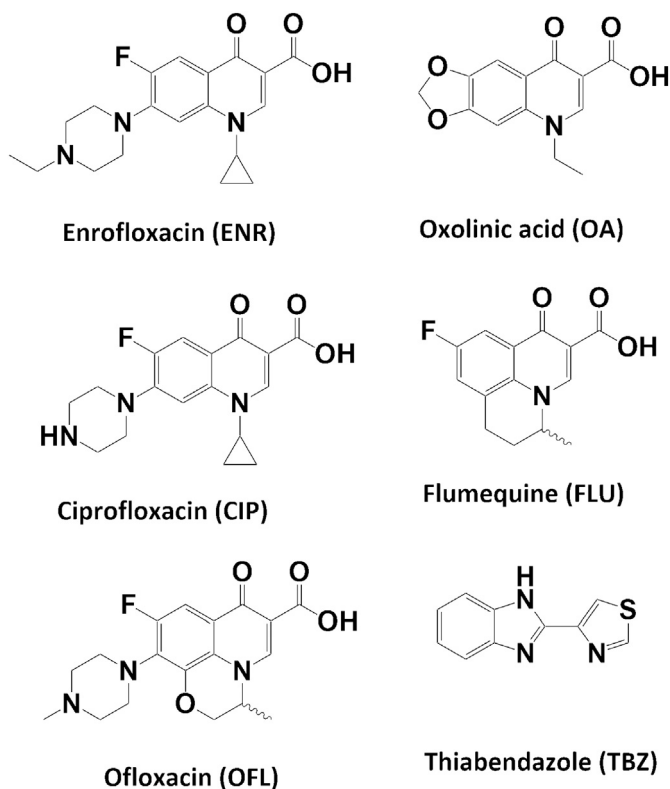


**Fig. 1.** Molecular structures from the employed contaminants.

Experiments were carried out employing the following matrices: i) ultra-pure water (MQ), ii) saline water, consisting of 30 g/L of NaCl in MQ (SW), and iii) simulated wastewater (SWW) prepared from MQ by adding the constituents shown in Table S1 (Michael et al., 2013). The initial pH was adjusted to 5.0 by the addition of diluted sulfuric acid; this pH is commonly employed for photo-Fenton under mild conditions (Gomis et al., 2015a). An additional experiment has been conducted in SWW without pH adjustment (ca. 7.5). Then, 100 µM of iron (as $FeSO_4 \cdot 7H_2O$) was added and consecutive additions of 5 mg/L of $H_2O_2$ were done at the beginning of the reaction and every 25 min. These are typical Fenton reagents concentrations employed in analogous works (Gomis et al., 2015b; Sciscenko et al., 2020). Experiments were carried out for 2 h, and samples were periodically taken to be analysed. Blank experiments, dark-Fenton, sunlight alone (with and without iron 100 µM) and $H_2O_2$-sunlight, were also performed in MQ at pH 5.0, and the respective results are shown in the Supporting Information, Fig. S1.

On the other hand, although several works that analyse the degradation of (F)Qs (Gou et al., 2021) (or other CECs able to chelate and, or even also reduce Fe(III) —such as phenolic compounds (Moreno-Andrés et al., 2021)—), the interaction iron-(F)Q is usually neglected, leading to plausible data misinterpretations, as it has been stated in a previous study (Sciscenko et al., 2021a). Therefore, we also decided to evaluate if the coexistence iron-(F)Q can enhance the degradation of a recalcitrant pollutant, choosing thiabendazole (TBZ) as probe CEC. TBZ is also fluorescent, thus being later on evaluated as a non-calibrated interference during PARAFAC modelling (differently from (F)Qs individual standards solutions, the individual TBZ solutions were not included into the dataset). In order to avoid the photolysis contribution, three dark-Fenton experiments in MQ at pH 5.0 were performed, one consisting of the aforementioned antibiotics mixture (ENR, OFL, CIP, OA and FLU, 3 µM each), another containing the 5 (F)Qs plus TBZ 3 µM, and TBZ 3 µM alone. The concentration of initial iron was reduced to 15 µM (1:1 stoichiometry respect to total (F)Qs), to obtain slower degradations (when employing $[Fe(II)]_0 = 100$ µM the desired effect was not observed due to iron excess). $H_2O_2$ addition rate of 5 mg/L each 25 min was kept as in solar-photo-Fenton experiments. The experiment was carried out in an open batch reactor containing 250 mL of testing solution and agitated with magnetic stirring, taking samples at different time intervals for 2 h. The reasons for changing to laboratory scale for these experiments were because removal kinetics results with dark-Fenton at laboratory and CPC reactor did not differ significantly, the sampling process was easier, and the assays required a lower volume of solution.

### 2.3. Sample preparation

Samples were always filtered with 0.45 µm PTFE filters (Chromafil Xtra). For HPLC measurements, methanol (final concentration 2.5 M) was added to the samples to stop the Fenton reaction due to $H_2O_2$ excess. On the other hand, for fluorescence spectroscopy determinations, addition of acetate/acetic acid buffer (pH = 4.5) was employed (final concentration 1.5 M of acetate + acetic acid), not only to stop the Fenton reaction, but also to keep similar measuring conditions between the different water matrices and reaction time-interval samples. It is widely reported that (F)Qs fluorescence is strongly pH dependent, having higher intensities in the pH range between 3 and 5 (Albini and Monti, 2003).

Since (F)Qs fluorescence can be quenched by Fe(III) (Sciscenko et al., 2021b), a comparison of EEM-PARAFAC models and score values obtained from samples also removing the iron (previous the EEM measurements), was performed. Differences between EEM fingerprints shapes, their maximum locations, scores initial values and respective kinetics trends, before and after iron removal, were negligible. However, samples were submitted to a pre-treatment to ensure complete iron elimination: pH was adjusted to pH 11, with NaOH 1 M, and filtered with the PTFE 0.45 µm filters; afterwards, the acetate/acetic acid buffer was added to reach the desired pH of 4.5.

## 2.4. Chemical analysis

Pollutants removal ((F)Qs and TBZ when present) were determined by HPLC analysis using a Hitachi Chromaster apparatus with a UV/Vis detector (model 5420) employing a C18 Machery-Nagel column Nucleodur-$\pi$2 (250 mm $\times$ 2 mm, 5 $\mu$m). The mobile phase flow was 0.25 mL/min, constituted by formic acid, acetonitrile and methanol, 80:7.5:12.5 (in %$v$/$v$), respectively, for the first 42 min in isocratic mode, and changing with gradient elution up to 20:50:30 until 70 min. TBZ, CIP, OFL and ENR were measured following the absorbance at 285 nm, whereas for FLU and OA 250 nm was used.

EEMs were measured in a Horiba PTI Quanta Master 400 spectrofluorometer, equipped with a Xe arc lamp, employing an excitation range of 250–400 nm (recorded with 5 nm intervals), and emission range from 300 to 600 nm (recorded within 2.5 nm intervals). Absorbance spectrums for inner filter effect corrections were measured with a Hitachi-UH5300 spectrophotometer. The same device was used to measure total iron and $H_2O_2$ concentrations based on ISO 6332:1988 standard method and the work of Nogueira et al. (2005), respectively.

PARAFAC modelling was performed with MATLAB 2020a, with the graphical user interface EEMlab developed in previous work (Micó et al., 2019). The dataset, which also included 3 EEM of each single (F)Q in concentrations from 0.5 to 3 $\mu$M, consisted of 127 absorbance spectra and EEM, respectively, as well as 14 blanks and 14 water Raman signals at 350 nm, the latter for intensity standardisation (Lawaetz and Stedmon, 2009). During the model preprocessing, 9 EEM were eliminated due to negligible fluorescence signal; primary Rayleigh scatter band was corrected with missing values, secondary Rayleigh, and both Raman scatter bands, were handled by interpolation; the emission axis was resized to 330–600 nm range. EEMs were always normalized to their total signal prior PARAFAC analysis, so that all fluorophores contained comparable weighting. Once the best model was chosen —that one containing all the components corresponding to parent pollutants and interferences, always keeping the chemical consistency—, normalization was reversed. For further details about EEM-PARAFAC processing steps and fundamentals, information can be found elsewhere (Bro, 1997; Murphy et al., 2013; Sciscenko et al., 2022).

For the dark-Fenton experiment, samples containing the 5 (F)Qs and the TBZ, the respective EEM were included in the aforementioned dataset, and PARAFAC modelling was carried out again. These samples were previously diluted by 1:3 factor due to the higher fluorescence quantum yield of TBZ. Differently from the (F)Qs, the EEM of TBZ standard solution was not uploaded into the dataset in order to be considered as a fluorescence interference. In this sense, SWW was never employed as blank, and its fluorescent DOM was an intrinsic interference as well.

## 2.5. Fe(III) speciation in ultra-pure and salty water

Due to the plausible formed complexes, a calculation based on published reported stability constants for ferric ions was carried out, as the efficiency of photo-Fenton is limited by Fe(III) reduction that is in turn ruled by its complexation. Calculations were performed employing MATLAB 2020a through "vpasolve" function ("MATLAB vpasolve", n.d.). Studied water matrices were MQ and SW, both at pH 5.0 containing 100 $\mu$M of Fe(III), with and without the 15 $\mu$M of total (F)Qs. Since the pH was 5.0, which is below the first pKa of the employed (F)Qs (see pKa values in Table S2), the antibiotics were expressed in their cationic form ($HFQ^+$), which is relevant for selecting the appropriate stability constants values.

The equilibrium concentrations were calculated employing the respective accumulative stability constants, $\beta_i$, (Eq. (2)), and the respective mass balances (Eqs. (3) and (4)) for total Fe(III) and ligands, respectively:

$$\beta_i = \frac{[Fe_x L_y^{3x-ym}]}{[Fe^{3+}]^x [L^m]^y} \tag{2}$$

$$[Fe_{total}] = [Fe^{3+}] + \sum x \, \beta_i \, [Fe^{3+}]^x [L^m]^y \tag{3}$$

$$[L_{total}] = [L^m] + \sum y \, \beta_i \, [Fe^{3+}]^x [L^m]^y \tag{4}$$

where $y$ and $m$ are the stoichiometry and charge number, respectively, of the ligand $L$ (i.e. $OH^-$, $Cl^-$ or $HFQ^+$), and $x$ is the stoichiometry number of $Fe^{3+}$ in the complex. Employed stability constants were: log$\beta$(Fe $(OH)^{2+}$) = $-2.19$ and $-2.79$ (according to ionic strength, values at MQ and SW, respectively); log$\beta$(Fe$(OH)_2^+$) = $-5.67$ and $-6.57$ (MQ and SW, respectively); log$\beta$(FeCl$^{2+}$) = 0.59; log$\beta$(FeCl$_2^+$) = 0.62; log$\beta$(FeHFQ$^{4+}$) = 18; log$\beta$(Fe(HFQ)$_2^{5+}$) = 27; log$\beta$(Fe(HFQ)$_3^{6+}$) = 39. Equilibrium constant values from Fe(III) hydrolysis, and of FeCl$^{2+}$ and FeCl$_2^+$ formation, were obtained from De Laat and Le (2006), whereas the ones for Fe(III)-(F)Qs complexes (estimated as an average) from Urbaniak and Kokot (2009).

# 3. Results and discussion

## 3.1. Water matrix effect: individual pollutants behaviour

Fast degradation, with comparable degradation rates, was obtained for all 5 pollutants in MQ, reaching 90 % removal with an $Q_{UV}$ = 2.5 kJ/L (Fig. 2A). Although the solar photo-Fenton process at pH 5.0 in MQ is usually slow due to iron precipitation, in the case of (F)Qs, Fenton-type processes are reported to be fast even at circumneutral conditions because of their ability to chelate Fe(III), forming photoactive complexes (Sciscenko et al., 2021a). Although Fe(II) complexes are less stable, they were described for some (F)Qs (Turel, 2002), and their formation, together with respective complexes formed with oxidation by-products, should not be ruled out. Moreover, despite their markedly different photolytic stability (discussed below), quinolones and FQs have comparable kinetic rate constants with HO• (An et al., 2010; Ge et al., 2015; Zhang et al., 2019). Since HO• generation is favoured in solar-photo-Fenton, this radical is expected to be the key reactive specie, and thus, similar removal rates are obtained, independently from the FQs chemical structure (Sciscenko et al., 2021b).

Blank experiments (degradation by sunlight alone, with and without iron, sunlight with $H_2O_2$ additions, and dark-Fenton) were also carried out in MQ pH 5.0 (see Fig. S1). The obtained photolytic degradation rate, OA $\geq$ FLU > OFL $\gg$ ENR = CIP (Fig. S1A), is in agreement with other works (Ge et al., 2015; Pouliquen et al., 2007; Zhang et al., 2019), correlated with the fact that the photolysis is dependent on the heterocycle electrophilicity, and that the absence of piperazine ring (reactive site) for FLU and OA, stabilises the molecule (Albini and Monti, 2003; Zhang and Huang, 2005). Interestingly, photolysis trends were changed in the presence of iron 100 $\mu$M (Fig. S1B), observing photolytic hindering for ENR and CIP, and enhancement of the less photolabile ones, OA, FLU and OFL (Fig. S1B), which is attributable to the different photostabilities of the formed (F)Qs-Fe(III) complexes (Hubicka et al., 2012; Sciscenko et al., 2021a; Serna-galvis et al., 2021). Hydrogen peroxide addition slightly accelerated (F)Qs removal rates (Fig. S1C), but the fastest kinetics were reached with dark-Fenton (Fig. S1D). However, these processes were clearly less efficient than solar-photo-Fenton: only 2.5 kJ/L —approximately 20 min treatment— were needed to reach nearly complete pollutant abatement, whereas for dark-Fenton, 120 min were required.

When changing the water matrix to SW pH 5.0, degradations were slower than with MQ and differences among pollutants removal rates could be observed: OA and FLU were the most recalcitrant, showing 75 % and 68 % removal with $Q_{UV} \approx$ 3.75 kJ/L, respectively, whereas for OFL was 87 %, and ENR and CIP was >95 % for the same dose of irradiation (Fig. 2B). The stability trend (OA/FLU > OFL > ENR/CIP) is consistent with the photolytic stability observed during the aforementioned photolysis experiment (Fig. S1A). This change in the trend compared with MQ is attributable to a less favoured generation of HO• by the photo-Fenton process, which results in a higher relative contribution of photolysis.

The lower efficiency of solar-photo-Fenton in SW might be attributed to HO• scavenging by $Cl^-$ (at pH 5.0, approximately 1 $\times$ 10$^5$ M$^{-1}$ s$^{-1}$ (Von Gunten, 2003)), and/or the formation of ferric-chloride complexes
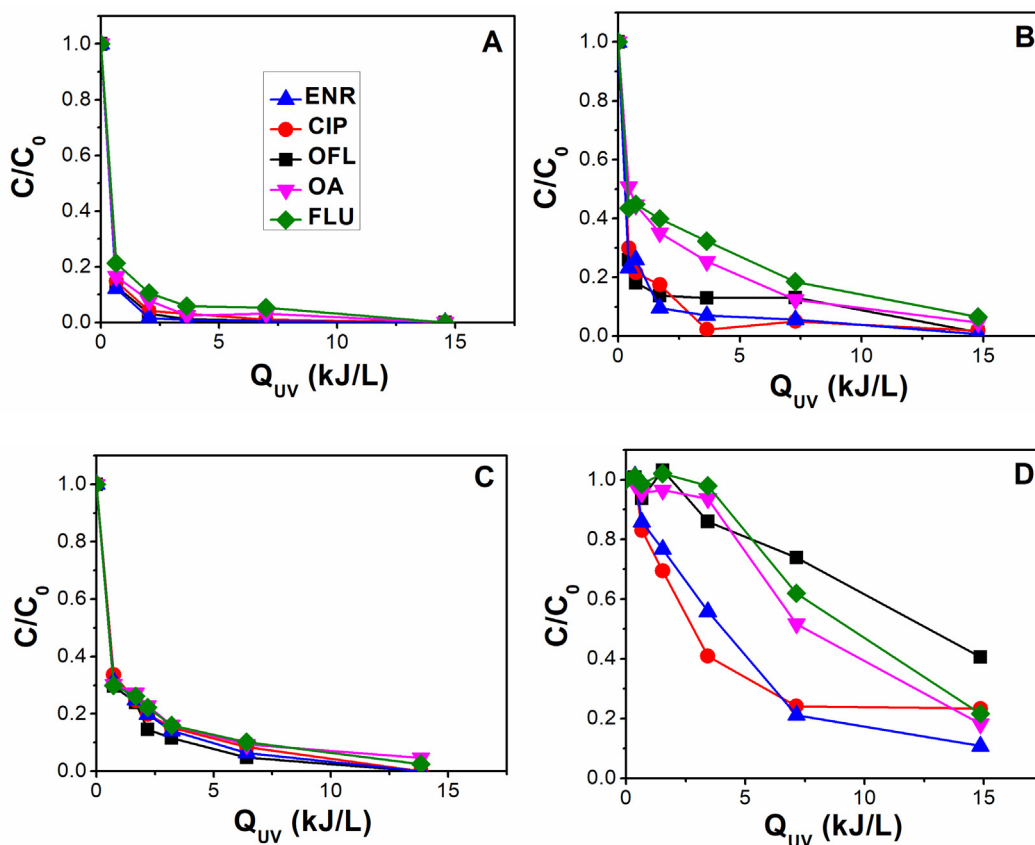
**Fig. 2.** Removal of (F)Qs, 3 μM each, by solar photo-Fenton ([Fe(II)]$_0$ = 100 μM and additions of [H$_2$O$_2$] = 5 mg/L every 25 min) in the different water matrices: A) MQ pH 5.0; B) SW pH 5.0; C) SWW pH 5.0; D) SWW natural pH = 7.5. Degradation expressed as normalized concentration (C/C$_0$) decay.

(FeCl$^{2+}$ and FeCl$_2^+$), which inhibit the Fenton-like step (Machulek et al., 2007). In order to confirm these hypotheses, iron speciation was calculated for 4 conditions: 100 μM of Fe(III) at pH 5.0, in MQ and SW, in the absence and the presence of the (F)Qs 15 μM (see Fig. 3). Interestingly, the single effect of 0.5 M of Cl$^-$ increases the Fe(OH)$^{2+}$ (a photoactive specie (Pignatello et al., 2006)) fraction in SW with respect to MQ, but the concentration of Fe(III)-chloride complexes is negligible (see Fig. 3A and B), therefore, no Fenton-like step inhibition is happening. When (F)Qs are present in MQ, 15 % of total iron is forming a 1:1 stoichiometry complex with the antibiotics, which involves that >99 % of the added pollutants are complexed with Fe(III). Interestingly, Fe(OH)$^{2+}$ concentration is also higher when (F)Qs are present than when they are not (compare Fig. 3A and C). Since the fraction of FeCl$^{2+}$ and FeCl$_2^+$ is negligible at pH 5.0, the results for the solutions containing (F)Qs in MQ or SW are analogous (see Fig. 3C and D) in both with comparable Fe(OH)$^{2+}$ percentages. In conclusion, the above-mentioned photo-Fenton efficiency loss in SW should be primarily attributed to the HO• scavenging role by chlorides.

In the case of SWW pH 5.0, comparable to MQ, the 5 (F)Qs exhibited similar degradation rates but were slightly slower than the latter, with overall 80 % degradation with Q$_{UV}$ = 2.5 kJ/L. In SWW we shall consider, on the one hand, the effect of DOM, and on the other, the presence of inorganic salts, in particular, phosphates (at pH 5.0, carbonate and bicarbonate concentrations are low), which might produce a certain grade of Fenton inhibition due to the formation of insoluble iron-phosphates salts (Pignatello et al., 2006). DOM plays an ambivalent role, acting as: i) HO• quencher and produce inner filter effect, thus decreasing the (F)Qs degradation produced by solar-photo-Fenton and photolysis; ii) photosensitiser (enhancing indirect photolysis by reactive oxygen species generation), as well as a chelating agent of iron, therefore, extending the pH-range where Fenton reaction is efficient (Gomis et al., 2014; Niu et al., 2016).

Finally, the experiment with SWW was run at unmodified pH (7.5–7.8). In this medium, Fenton inactivation via the formation of iron oxides and/or hydroxides becomes critical, resulting in a worse process performance. Moreover, besides the phosphates effect, the presence of (bi)carbonates at this pH shall play a markedly negative influence due to HO• quenching (1 × 10$^7$–1 × 10$^8$ M$^{-1}$ s$^{-1}$ (Buxton et al., 1988)). In spite of these issues, a significant degree of degradation was observed, being at Q$_{UV}$ ≈ 7.5 kJ/L, 75 % removal for ENR and CIP, 50 % for OA, 40 % for FLU and 25 % for OFL (Fig. 2D). General trends in reactivity described for SW are here observed, except for OFL, which suffered the slowest degradation, most probably due to different interactions of this compound (which shows the highest polarity) with the matrix constituents, such as cations or organic matter (Cuprys et al., 2018).

### 3.2. Selection of the PARAFAC model

The normalized EEM for each (F)Q was measured (Fig. 4A). The observable fluorescence maxima were as follows: ENR and CIP, with practically identical fingerprints, at λ$_{ex}$ = 273 nm and λ$_{em}$ = 450 nm, excitation and emission wavelengths, respectively; OFL with λ$_{ex}$ = 295 nm and λ$_{em}$ = 510 nm; OA with λ$_{ex}$ ≤ 250 nm and λ$_{em}$ = 375 nm; FLU with λ$_{ex}$ ≤ 250 nm and λ$_{em}$ = 360 nm. In Fig. S2 some of the recorded normalized EEM shape changes during solar-photo-Fenton in different water matrices are shown as examples.

A 6-component PARAFAC model was chosen as the best to describe the whole dataset. As shown in Fig. 4B, components C2, C3 and C4 perfectly fit with the fingerprints of OFL, OA and FLU, respectively. On the other hand, component C1 fits with the one of ENR and CIP, due to their analogous EEM. In this sense, the aforementioned components will also consider fluorescence intensity coming from generated by-products with similar
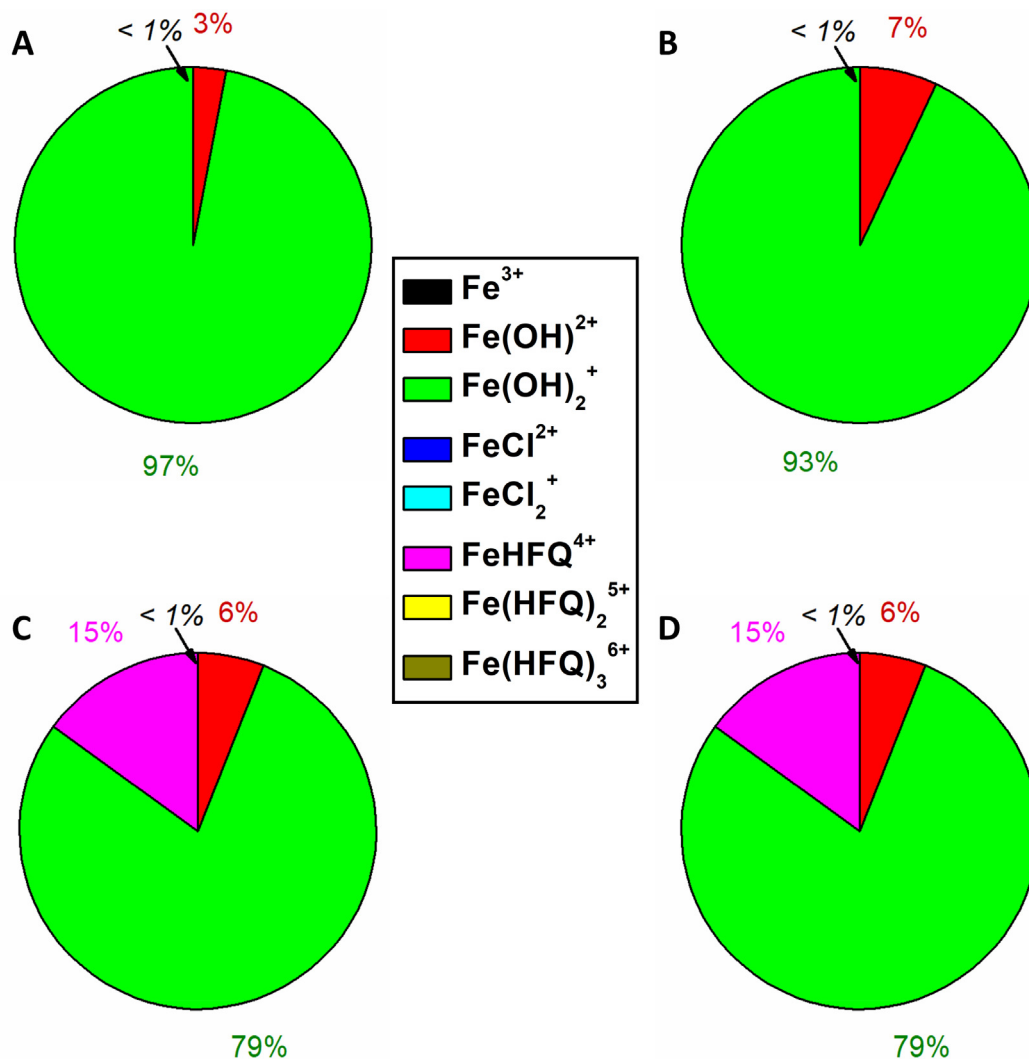
**Fig. 3.** Estimation of Fe(III) 100 μM speciation at pH 5.0 in. A) ultra-pure water (MQ); B) salty water (SW); C) MQ with (F)Qs; D) SW with (F)Qs.

EEM fingerprints to the parent pollutants (e.g. due to slight structural changes, such as a hydroxylation or an alkyl moiety cleavage). In fact, CIP is reported as a major photoproduct of ENR (Sciscenko et al., 2021a; Snowberger et al., 2016). For this reason, C1 gathers each ENR-like species, C2 the OFL-like family, C3 the OA-like and C4 the FLU-like.

The other two components, X1 and X2, belong to non-calibrated substances. By comparison with C1, X1 (fluorescence maximum at $\lambda_{ex} = 270$ nm and $\lambda_{em} = 435$ nm) might be assigned to transformation products with comparable molecular structures to ENR and CIP. In fact, X1 component was also detected in a previous work while degrading ENR alone with photo-Fenton employing simulated sunlight (Sciscenko et al., 2020). On the other hand, transformation products emitting within the X2 region exhibit its excitation maximum at wavelengths <250 nm and emission at 460 nm, which might represent deeper structural changes, a component also found in previous studies (Sciscenko et al., 2021b, 2020). In addition, humic-like substances, only present in SWW, emit in the region contained in X2 and thus, are included in this component (Henderson et al., 2009; Murphy et al., 2011).

Considering only the EEM from pure standards (Fig. 4A) at different concentrations (0.5 to 3 μM), calibration curves were obtained for each antibiotic (plot of scores vs. concentration); results can be found in Table 1. Detection limits, clearly below 0.5 μM, were obtained in all cases. Differences among (F)Qs fluorescence quantum yields can also be observed by the obtained sensitivities (calibration curves slopes), the lowest being for FLU with $8.9 \pm 0.2$ μM$^{-1}$ and the highest for ENR with $37.6 \pm 0.8$ μM$^{-1}$, in line with other works (Albini and Monti, 2003).

*3.3. PARAFAC components trends*

Scores (i.e. fluorescence intensity (Murphy et al., 2013)) from components C1–C4 were plotted vs. $Q_{UV}$ for each treatment, being normalized by their value at $Q_{UV} = 0$ kJ/L (Fig. 5), allowing to observe the behaviour of ENR-like, OA-like, OFL-like and FLU-like throughout the processes.

A comparison between Fig. 5 and Fig. 2 indicates that the total fluorescence trends are in line with the previously observed degradation rates, being: MQ (pH = 5.0) > SWW (pH = 5.0) > SW (pH = 5.0) > SWW (pH = 7.5). As expected, scores from C1–C4 components exhibited slightly slower decay than the pollutants individual chromatographic areas due to the contribution of by-products to the overall fluorescence. For instance, FLU-like (C4) had a decay of 80 % with $Q_{UV} = 2.5$ kJ/L in MQ (Fig. 5A), whereas FLU removal was 90 % with the same $Q_{UV}$ according to the HPLC-UV/vis measurements (Fig. 2A).

Interestingly in SW (Fig. 5B), most of the fluorescent generated by-products can be labelled as OA-like, in agreement with the $Q_{UV}$-profile of C3 component: a fast decay in the early stages of the process (also observed for the other 3 components due to the fast Fenton step) followed by a *plateau* behaviour. As OA is efficiently removed by photo-Fenton (Fig. 2B), the existence of the *plateau* region could only be explained if
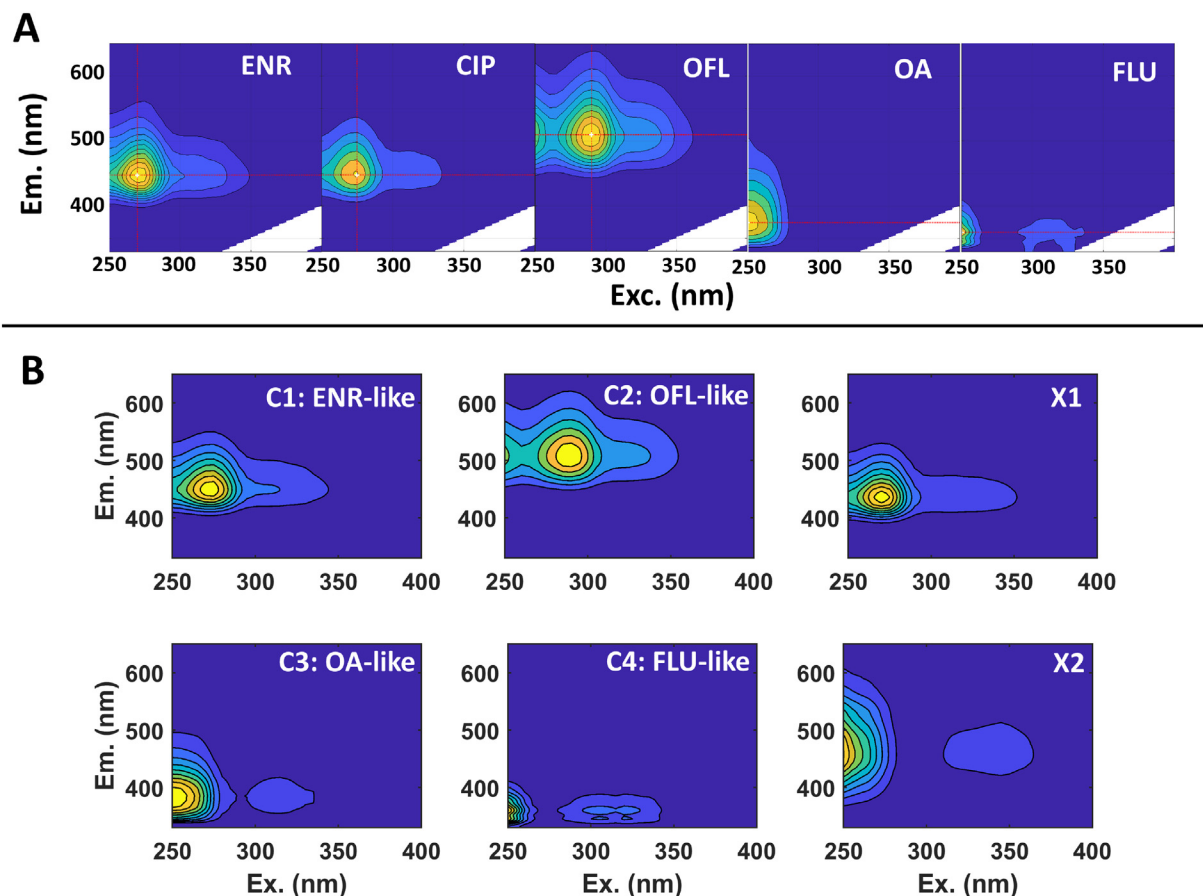
**Fig. 4.** A) Normalized EEM from the (F)Qs individual standard solutions; B) PARAFAC 6-component model: parent pollutants fingerprints (components C1 to C4), and detected interferences (components X1 and X2).

some of the generated by-products have their fluorescence emission within OA-like fingerprint. Although the nature of these components could only be unequivocally determined by HPLC-MS analysis, which is beyond the aim of this work, it can be hypothesised that substitution of fluorides and piperazine moieties by hydroxyl groups could occur in initial steps of the oxidative process, to give molecular structures more similar to OA (see Fig. 1). Contribution from chlorinated by-products should not be disregarded (reported second-order rate constants for (F)Qs are significant, being approximately $1 \times 10^{10}$ M$^{-1}$ s$^{-1}$ with Cl• and $2 \times 10^{8}$ M$^{-1}$ s$^{-1}$ with Cl$_2$$^{•-}$ (Lei et al., 2019)).

For SWW at pH 5.0, PARAFAC components scores (Fig. 5C) showed the same trend as the observed for the individual pollutants. However, at pH 7.5, most of the generated by-products are ENR-like, since ENR and CIP removals were 80 %, respectively, with $Q_{UV} \approx 7.5$ kJ/L (see Fig. 2D), whereas C1 score-values only exhibited a 30 % decay in the same period (Fig. 5D). Following the explanation given for SW, accumulation of ENR-like by-products indicate the deficient destruction of the molecule, indicating that in this case, fluoride and piperazine might remain in the by-

products structure, in line with the lower efficiency of photo-Fenton in these conditions.

The scores from components X1 and X2 were also plotted (Fig. 6). X1 appeared in each water matrix, showing a kinetic behaviour that can be associated with reaction intermediates: an initial increase followed by a subsequent decrease (Fig. 6A). In agreement with slower degradation kinetics, X1 accumulation was higher in SWW pH 7.5 than at pH 5.0; one can see that at $Q_{UV} = 3$ kJ/L, X1's score values in SWW natural pH were the double than the ones at pH 5.0. Moreover, although straight comparisons cannot be made among fluorescent behaviors within different water matrices, at pH 5.0, the persistence of X1 in MQ was shorter than in SWW, and the highest accumulation was observed in SW, with a notable maximum within the first $Q_{UV}$-values. As previously mentioned, intermediates in SW could also be chlorinated compounds.

When analysing X2 scores (Fig. 6B), for initial samples ($Q_{UV} = 0$ kJ/L), it was negligible in MQ and SW, but significant in SWW at both pH. As discussed in the previous section, this is attributable to the presence of humic-like substances, whose signal is included in X2 fingerprint. In agreement with this, X2-scores followed a "by-product behaviour" only in MQ and SW (an initial increase and then a decrease), whereas in SWW, the trends were more complex: a first fast decay, due to DOM removal, with a subsequent increase due to oxidation intermediates formation. The final fluorescence of X2 was four times higher in SWW pH 7.5 than at pH 5.0, in line with the faster degradation kinetics for the latter.

### 3.4. Thiabendazole degradation in presence of (fluoro)quinolones

In order to go further into the complexity of the system, an extra CEC, namely thiabendazole (TBZ), was added to the system. As explained in
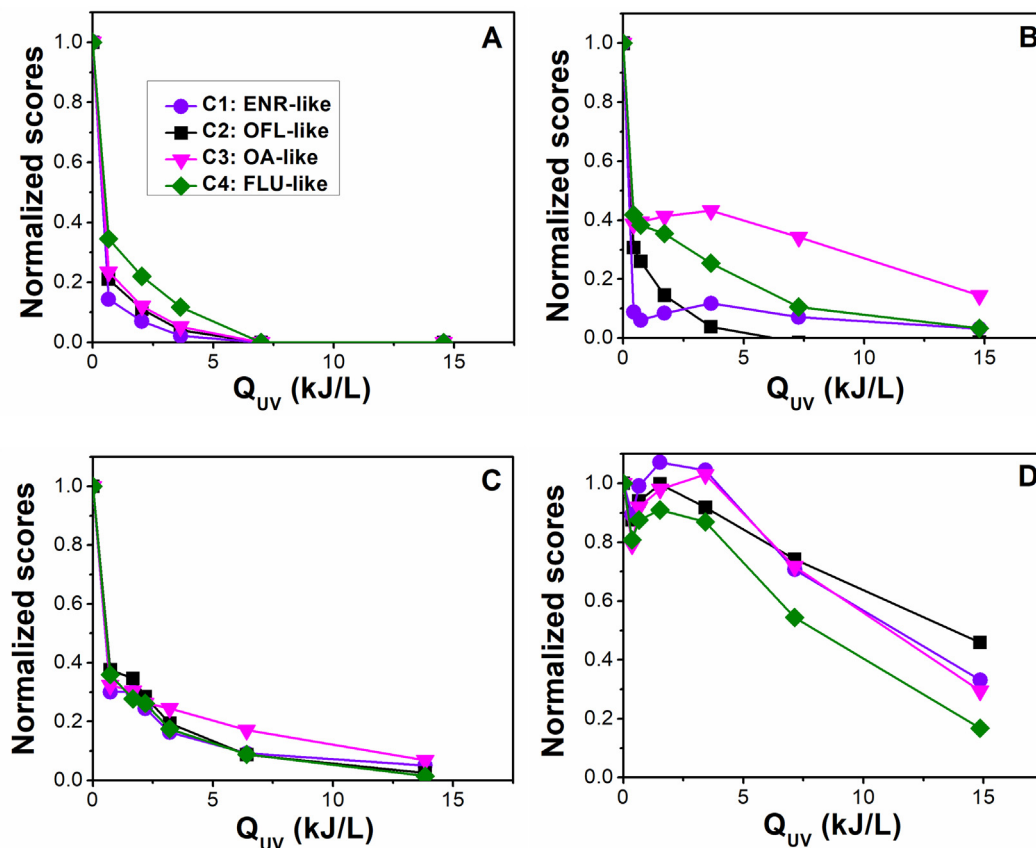
**Table 1**
Least squares regressions employing the obtained 6-component PARAFAC model to measure the scores from (F)Qs standard solutions.

| Compound | Slope (μM$^{-1}$) | Detection limit (μM) |
|---|---|---|
| ENR | 37.6 ± 0.8 | 0.23 ± 0.03 |
| CIP | 21.4 ± 0.6 | 0.02 ± 0.05 |
| OFL | 33.3 ± 0.6 | 0.10 ± 0.03 |
| OA | 20.5 ± 0.4 | 0.10 ± 0.05 |
| FLU | 8.9 ± 0.2 | 0.2 ± 0.4 |

**Fig. 5.** Normalized scores behaviour from the PARAFAC components, ENR-like, OFL-like, OA-like and FLU-like, during the removal of (F)Qs, 3 μM each, by solar photo-Fenton ([Fe(II)]$_0$ = 100 μM and additions of [H$_2$O$_2$] = 5 mg/L every 25 min) in: A) MQ pH 5.0; B) SW pH 5.0; C) SWW pH 5.0; D) SWW natural pH (≈7.5).

Section 2.2, the solution consisted of all 5 (F)Qs (each at 3 μM concentration), TBZ (also 3 μM), 15 μM of initial Fe(II), pH = 5.0 and the additions of 5 mg/L of H$_2$O$_2$ every 25 min. For the sake of comparison, the reaction was performed under the same conditions in the absence of (F)Qs, and a control experiment only containing the (F)Qs mixture (without TBZ). Dark-Fenton was employed in order to avoid the effect of pollutants photolysis and obtain slower reactions, which allows a more accurate analysis.

TBZ removal was >90 % in 120 min in the presence of (F)Qs, but only of 50 % in its absence (Fig. 7). These results indicate that in order to compensate the competitive role of (F)Qs for the reactive species, an enhancement of the Fenton system must occur, attributable to the formation of stable Fe

(III)-FQ complexes (Efthimiadou et al., 2008; Sciscenko et al., 2021a), which is evidenced with the initial and final concentrations of dissolved total iron in each case: in the presence of (F)Qs, the initial concentration of total iron was 15.1 μM whereas without them was 9.6 μM; after the 2 h of treatment, the respective final concentrations were 7.3 and 1.3 μM, indicating that formed by-products from (F)Qs shall chelate iron as well. Moreover, besides keeping iron dissolved at pH 5.0, (F)Qs might also help to accelerate Fe(III) reduction, which is the limiting step of the Fenton reaction. This result is certainly of interest when studying the fate of complex mixtures of CECs in the presence of (F)Qs with Fenton-related processes (at least with comparable concentrations to the ones in this work).
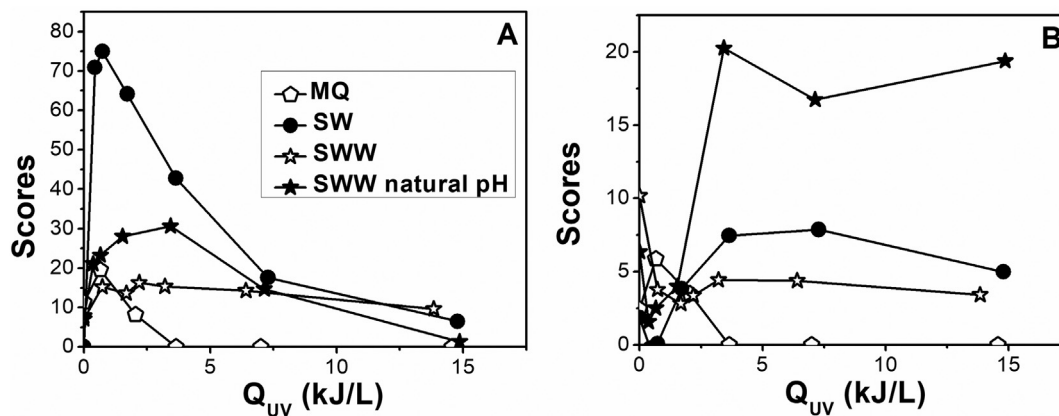


**Fig. 6.** Scores behaviour from the PARAFAC components corresponding to non-calibrated substances, A) X1 and B) X2, in the different studied water matrices.
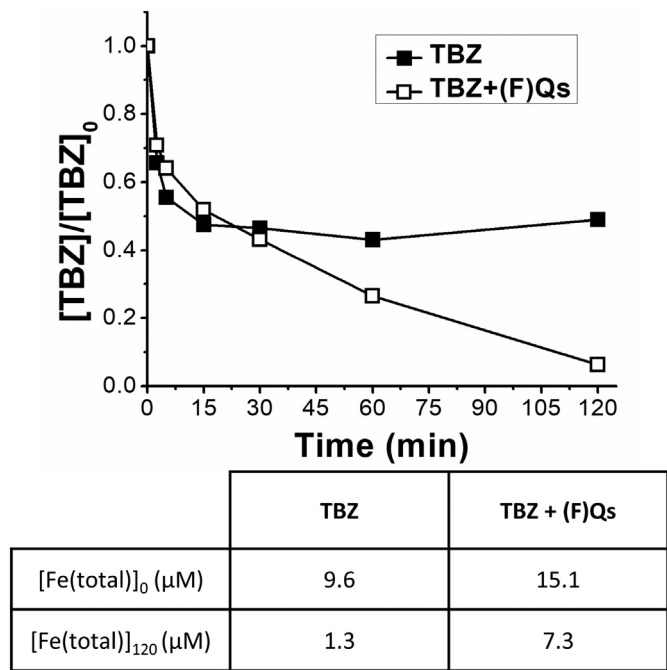
**Fig. 7.** Dark-Fenton treatment of TBZ 3 μM in MQ at pH 5.0, employing 15 μM of Fe (II) and 5 mg/L each 25 min dosage of $H_2O_2$, in absence and presence of the (F)Qs mixture (OFL, CIP, ENR, OA and FLU, each in concentration of 3 μM). Inserted in the figure, a table with initial and final total iron concentrations for each case.

The EEM resulting from the reactions containing (F)Qs and TBZ were included in the dataset in order to test if TBZ fingerprint is deconvoluted without interfering with the previously obtained components. Differently from the (F)Qs, it has to be remarked that TBZ was not calibrated, as EEM of TBZ standard solutions or TBZ individual degradation were not introduced into the dataset. Interestingly, a 7-component PARAFAC model was obtained now, which consists of C1–C4, X1 and X2, plus the one corresponding to TBZ-like substances (Fig. 8).

Accordingly, scores time-variation during the dark-Fenton reaction is represented in Fig. 9A. Expected trends were obtained: decreases of ENR,

OFL, OA and FLU-like components could still be observed, but also for the TBZ-like component, and an increase for X1 with a subsequent *plateau*. X2 scores were only appreciated at the end of the reaction. These results mean that the EEM-PARAFAC can be a useful tool to monitor the behaviour of pollutants, grouped by structural similarity, at low concentrations and even in the presence of unidentified species, in this case, TBZ (water matrix strong interference) and released by-products (X1 and X2).

The same PARAFAC model was employed to measure the scores trend of the control experiment (analogous dark-Fenton of (F)Qs alone without the TBZ), results shown in Fig. 9B. Comparing Fig. 9A and B, we can mention that in the last case: i) scores from the C1–C4 exhibited faster decay (negligible fluorescence after 60 min), ii) X1 scores reached a lower maximum with a subsequent decay after 15 min instead of a *plateau*, and iii) as a proof of good modelling, TBZ-like scores were zero in the initial sample, and no by-products emitting within TBZ-like fingerprint are formed. These results are in agreement with the fact that in the control experiment, there is no TBZ competing for HO•, therefore, (F)Qs are consumed faster and the formed by-products exhibit a shorter persistence.

## 4. Conclusions

A methodology based on fluorescence has been tested to study the treatment of a (F)Q mixture by (photo-)Fenton processes in diverse aqueous matrices and at a CPC pilot plant. Despite the high similarity of the pollutants molecular structures, EEM fingerprints from four of them were deconvoluted. This allowed gathering (F)Qs and interferences within a 6 component PARAFAC model: ENR-like species (also including CIP), OFL-like, OA-like, FLU-like, and two families of by-products, one still showing quinolonic characteristics (X1), and another associated to DOM (present in SWW) plus another oxidised substances (X2). When an additional specie was added (TBZ), besides the aforementioned components, PARAFAC was able to add a TBZ-like component as well. This proves that only with an affordable instrumentation, an improved monitoring of the process can be reached when compared with routine chromatographic tools. This could be a key finding in order to develop a low-cost methodology for the analysis of selected CECs without calibration in real effluents.

The EEM-PARAFAC methodology could be extrapolated to other research fields studying (F)Qs (photo)chemical processes, such as medicine or fine chemistry, as well as for the analysis of other fluorescent CECs. In this context, for pollutants exhibiting higher fluorescence quantum yield
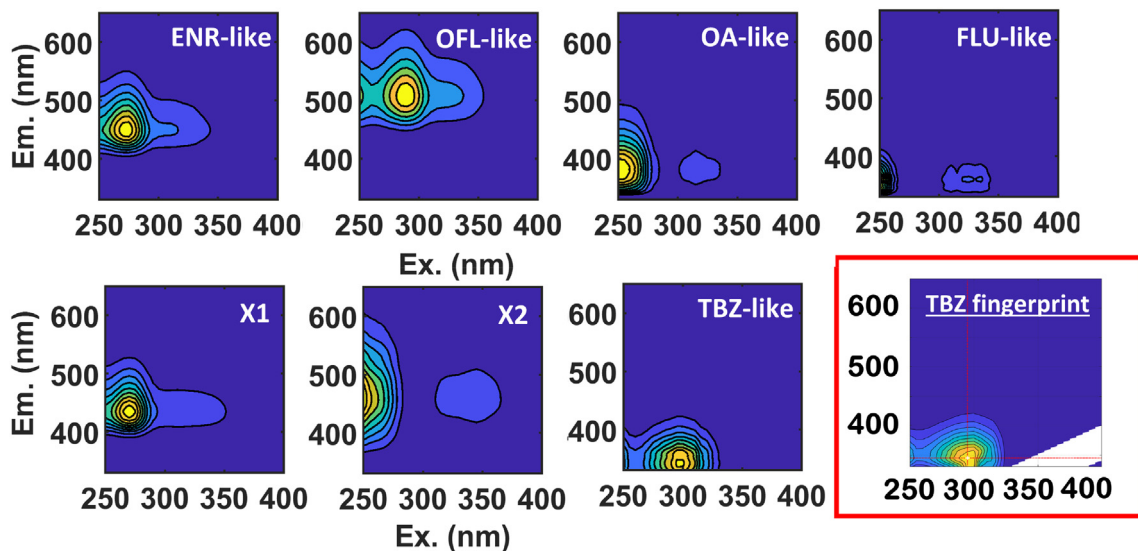


**Fig. 8.** PARAFAC model of 7 components by adding the EEM from dark-Fenton degradation of TBZ 3 μM in presence of the 5 (F)Qs to the previous dataset. The EEM of TBZ standard solution is also given for comparison with TBZ-like component, but it was not introduced in the dataset.
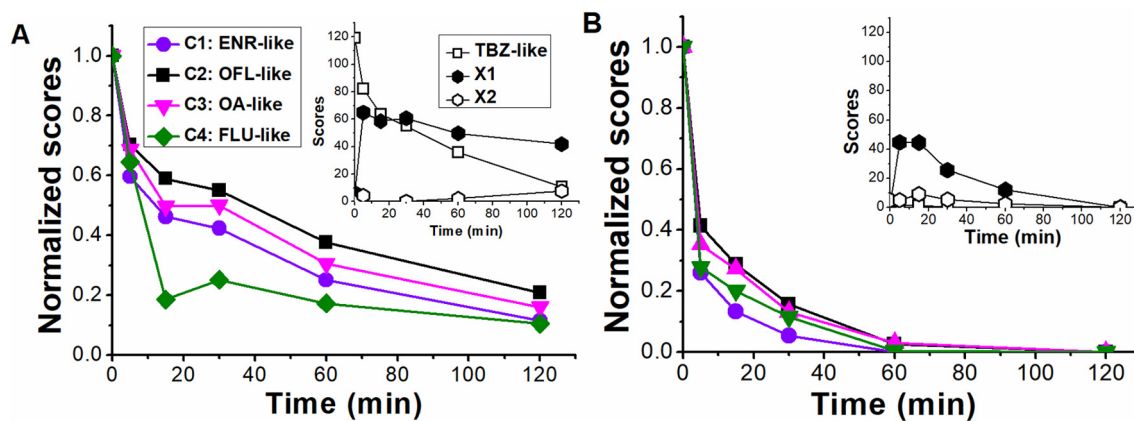
**Fig. 9.** Normalized scores during dark-Fenton treatment ([Fe(II)]$_0$ = 15 μM and additions of 5 mg/L of H$_2$O$_2$ every 25 min) employing EEM-PARAFAC model containing the TBZ-like component for the solutions: A) (F)Qs 15 μM with TBZ 3 μM; B) (F)Qs 15 μM. Inserted in each graph, the respective scores trends from the interferences, TBZ-like, X1 and X2.

than (F)Qs, detection limits within the ng/L–μg/L range should be easily achieved, as it was of a few μg/L for these antibiotics.

The solar photo-Fenton treatment of the (F)Qs mixture is clearly ruled by iron complexation. In conditions favoring efficient HO• generation (MQ and SWW at pH 5.0), similar removal rates were observed for all 5 compounds, photolysis contribution only becoming more important when the HO• scavenging is significant (SW at pH 5.0 and SWW at pH 7.5). In addition, the (F)Q-Fe(III) can play a major role in (photo-)Fenton processes at pH = 5, as shown by the enhanced TBZ removal in the presence of these antibiotics. This is an important result of plausible cross-effect between CECs when they are treated by Fenton-related systems. Moreover, iron speciation calculations at different pH values, presence of ligands, such as dissolved organic matter, CECs or anions, could be of interest to predict and/or explain the efficiency of a photo-Fenton treatment (i.e. analysing the change in concentration of FeOH$^{2+}$ and fraction of chelated iron).

Finally, in order to verify the hypothesis made in this work (formation of by-products with double hydroxylation replacing fluoride and piperazine ring, as well as plausible chloride addition to quinolonic ring in the case of SW) correlating EEM-PARAFAC with mass spectrometry is certainly an interesting task to perform in future work to fully understand the advantages and weaknesses that this multivariate analysis approach has.

## CRediT authorship contribution statement

**Iván Sciscenko**: Conceptualization, Methodology, Investigation, Writing – Original Draft, Writing – Review and Editing. **Margarita Mora**: Software, Writing – Review and Editing. **Pau Micó**: Software, Writing – Review and Editing. **Carlos Escudero-Oñate**: Supervision, Writing – Review and Editing. **Isabel Oller**: Supervision, Writing – Review and Editing. **Antonio Arques**: Conceptualization, Supervision, Funding acquisition, Writing – Review and Editing.

## Declaration of competing interest

The authors declare that they have no known competing financial interests or personal relationships that could have appeared to influence the work reported in this paper.

## Acknowledgements

## Appendix A. Supplementary data

Supplementary data to this article can be found online at https://doi.org/10.1016/j.scitotenv.2022.158338.

## References

Albini, A., Monti, S., 2003. Photophysics and photochemistry of fluoroquinolones. Chem. Soc. Rev. 32, 238–250. https://doi.org/10.1039/b209220b.

An, T., Yang, H., Song, W., Li, G., Luo, H., Cooper, W.J., 2010. Mechanistic considerations for the advanced oxidation treatment of fluoroquinolone pharmaceutical compounds using TiO2 heterogeneous catalysis. J. Phys. Chem. A 114, 2569–2575. https://doi.org/10.1021/jp911349y.

Bokare, A.D., Choi, W., 2014. Review of iron-free Fenton-like systems for activating H2O2 in advanced oxidation processes. J. Hazard. Mater. 275, 121–135. https://doi.org/10.1016/j.jhazmat.2014.04.054.

Bro, R., 1997. PARAFAC. Tutorial and applications. Chemom. Intell. Lab. Syst. 38, 149–171. https://doi.org/10.1016/S0169-7439(97)00032-4.

Buxton, G.V., Greenstock, C.L., Helman, W.P., Ross, A.B., 1988. Critical review of rate constants for reactions of hydrated electrons, hydrogen atoms and hydroxyl radicals (·OH/·O −) in aqueous solution. J. Phys. Chem. Ref. Data 17, 513–886. https://doi.org/10.1063/1.555805.

Carabajal, M.D., Arancibia, J.A., Escandar, G.M., 2017. Excitation-emission fluorescence-kinetic data obtained by Fenton degradation. Determination of heavy-polycyclic aromatic hydrocarbons by four-way parallel factor analysis. Talanta 165, 52–63. https://doi.org/10.1016/j.talanta.2016.12.030.

Carra, I., Malato, S., Jiménez, M., Maldonado, M.I., Sánchez Pérez, J.A., 2014. Microcontaminant removal by solar photo-Fenton at natural pH run with sequential and continuous iron additions. Chem. Eng. J. 235, 132–140. https://doi.org/10.1016/j.cej.2013.09.029.

Cui, H., Zhao, Y., Zhao, L., Wei, Z., 2022. Characterization of mercury binding to different molecular weight fractions of dissolved organic matter. J. Hazard. Mater. 431, 128593. https://doi.org/10.1016/j.jhazmat.2022.128593.

Cuprys, A., Pulicharla, R., Brar, S.K., Drogui, P., Verma, M., Surampalli, R.Y., 2018. Fluoroquinolones metal complexation and its environmental impacts. Coord. Chem. Rev. 376, 46–61. https://doi.org/10.1016/j.ccr.2018.05.019.

De Laat, J., Le, T.G., 2006. Effects of chloride ions on the iron(III)-catalyzed decomposition of hydrogen peroxide and on the efficiency of the Fenton-like oxidation process. Appl. Catal. B Environ. 66, 137–146. https://doi.org/10.1016/j.apcatb.2006.03.008.

Delalay, G., Berezowski, J.A., Diserens, N., Schmidt-Posthaus, H., 2020. An understated danger: antimicrobial resistance in aquaculture and pet fish in Switzerland, a retrospective study from 2000 to 2017. J. Fish Dis. 43, 1299–1315. https://doi.org/10.1111/jfd.13234.

Efthimiadou, E.K., Karaliota, A., Psomas, G., 2008. Mononuclear metal complexes of the second-generation quinolone antibacterial agent enrofloxacin: synthesis, structure, antibacterial activity and interaction with DNA. Polyhedron 27, 1729–1738. https://doi.org/10.1016/j.poly.2008.02.006.

Ezzariai, A., Hafidi, M., Khadra, A., Aemig, Q., El Fels, L., Barret, M., Merlina, G., Patureau, D., Pinelli, E., 2018. Human and veterinary antibiotics during composting of sludge or manure: global perspectives on persistence, degradation, and resistance genes. J. Hazard. Mater. 359, 465–481. https://doi.org/10.1016/j.jhazmat.2018.07.092.

Feng, M., Wang, Z., Dionysiou, D.D., Sharma, V.K., 2018. Metal-mediated oxidation of fluoroquinolone antibiotics in water: a review on kinetics, transformation products, and toxicity assessment. J. Hazard. Mater. 344, 1136–1154. https://doi.org/10.1016/j.jhazmat.2017.08.067.

Ge, L., Na, G., Zhang, S., Li, K., Zhang, P., Ren, H., Yao, Z., 2015. New insights into the aquatic photochemistry of fluoroquinolone antibiotics: direct photodegradation, hydroxyl-radical oxidation, and antibacterial activity changes. Sci. Total Environ. 527–528, 12–17. https://doi.org/10.1016/j.scitotenv.2015.04.099.

Gomis, J., Bianco Prevot, A., Montoneri, E., González, M.C., Amat, A.M., Mártire, D.O., Arques, A., Carlos, L., 2014. Waste sourced bio-based substances for solar-driven waste-water remediation: photodegradation of emerging pollutants. Chem. Eng. J. 235, 236–243. https://doi.org/10.1016/j.cej.2013.09.009.

Gomis, J., Carlos, L., Prevot, A.B., Teixeira, A.C.S.C., Mora, M., Amat, A.M., Vicente, R., Arques, A., 2015. Bio-based substances from urban waste as auxiliaries for solar photo-Fenton treatment under mild conditions: optimization of operational variables. Catal. Today 240, 39–45. https://doi.org/10.1016/j.cattod.2014.03.034.

Gomis, Juan, Gonçalves, M.G., Vercher, R.F., Sabater, C., Castillo, M.A., Prevot, A.B., Amat, A.M., Arques, A., 2015. Determination of photostability, biocompatibility and efficiency as photo-Fenton auxiliaries of three different types of soluble bio-based substances (SBO). Catal. Today 252, 177–183. https://doi.org/10.1016/j.cattod.2014.10.015.

Gou, Y., Chen, P., Yang, L., Li, S., Peng, L., Song, S., Xu, Y., 2021. Degradation of fluoroquinolones in homogeneous and heterogeneous photo-Fenton processes: a review. Chemosphere 270, 129481. https://doi.org/10.1016/j.chemosphere.2020.129481.

Grebel, J.E., Pignatello, J.J., Mitch, W.A., 2010. Effect of halide ions and carbonates on organic contaminant degradation by hydroxyl radical-based advanced oxidation processes in saline waters. Environ. Sci. Technol. 44, 6822–6828. https://doi.org/10.1021/es1010225.

Henderson, R.K., Baker, A., Murphy, K.R., Hambly, A., Stuetz, R.M., Khan, S.J., 2009. Fluorescence as a potential monitoring tool for recycled water systems: a review. Water Res. 43, 863–881. https://doi.org/10.1016/j.watres.2008.11.027.

Hubicka, U., Krzek, J., Zuromska, B., Walczak, M., Zylewski, M., Pawłowski, D., 2012. Determination of photostability and photodegradation products of moxifloxacin in the presence of metal ions in solutions and solid phase. Kinetics and identification of photoproducts. Photochem. Photobiol. Sci. 11, 351–357. https://doi.org/10.1039/c1pp05259d.

Hughes, S.R., Kay, P., Brown, L.E., 2013. Global synthesis and critical evaluation of pharmaceutical data sets collected from river systems. Environ. Sci. Technol. 47, 661–677. https://doi.org/10.1021/es3030148.

Lawaetz, A.J., Stedmon, C.A., 2009. Fluorescence intensity calibration using the raman scatter peak of water. Appl. Spectrosc. 63, 936–940. https://doi.org/10.1366/000370209788964548.

Lei, Y., Cheng, S., Luo, N., Yang, X., An, T., 2019. Rate constants and mechanisms of the reactions of Cl• and Cl2•- with trace organic contaminants. Environ. Sci. Technol. https://doi.org/10.1021/acs.est.9b02462.

Lin, R., Li, Y., Yong, T., Cao, W., Wu, J., Shen, Y., 2022. Synergistic effects of oxidation, coagulation and adsorption in the integrated Fenton-based process for wastewater treatment: a review. J. Environ. Manag. 306, 114460. https://doi.org/10.1016/j.jenvman.2022.114460.

Lu, S., Lin, C., Lei, K., Wang, B., Xin, M., Gu, X., Cao, Y., Liu, X., Ouyang, W., He, M., 2020. Occurrence, spatiotemporal variation, and ecological risk of antibiotics in the water of the semi-enclosed urbanized Jiaozhou Bay in eastern China. Water Res. 184, 116187. https://doi.org/10.1016/j.watres.2020.116187.

Machulek, A., Moraes, J.E.F., Vautier-Giongo, C., Silverio, C.A., Friedrich, L.C., Nascimento, C.A.O., Gonzalez, M.C., Quina, F.H., 2007. Abatement of the inhibitory effect of chloride anions on the photo-Fenton process. Environ. Sci. Technol. 41, 8459–8463. https://doi.org/10.1021/es071884q.

Malato, S., Fernández-Ibáñez, P., Maldonado, M.I., Blanco, J., Gernjak, W., 2009. Decontamination and disinfection of water by solar photocatalysis: recent overview and trends. Catal. Today 147, 1–59. https://doi.org/10.1016/j.cattod.2009.06.018.

MATLAB vpasolve, URL https://es.mathworks.com/help/symbolic/sym.vpasolve.html. (Accessed 13 July 2022).

Michael, I., Hapeshi, E., Aceña, J., Perez, S., Petrović, M., Zapata, A., Barceló, D., Malato, S., Fatta-Kassinos, D., 2013. Light-induced catalytic transformation of ofloxacin by solar Fenton in various water matrices at a pilot plant: mineralization and characterization of major intermediate products. Sci. Total Environ. 461–462, 39–48. https://doi.org/10.1016/j.scitotenv.2013.04.054.

Micó, P., García-Ballesteros, S., Mora, M., Vicente, R., Amat, A.M., Arques, A., 2019. EEMlab: a graphical user-friendly interface for fluorimetry experiments based on the drEEM toolbox. Chemom. Intell. Lab. Syst. 188, 6–13. https://doi.org/10.1016/j.chemolab.2019.03.001.

Moreno-Andrés, J., Farinango, G., Romero-Martínez, L., Acevedo-Merino, A., Nebot, E., 2019. Application of persulfate salts for enhancing UV disinfection in marine waters. Water Res. 163. https://doi.org/10.1016/j.watres.2019.114866.

Moreno-Andrés, J., Vallés, I., García-Negueroles, P., Santos-Juanes, L., Arques, A., 2021. Enhancement of iron-based photo-driven processes by the presence of catechol moieties. Catalysts 11, 1–15. https://doi.org/10.3390/catal11030372.

Murphy, K.R., Hambly, A., Singh, S., Henderson, R.K., Baker, A., Stuetz, R., Khan, S.J., 2011. Organic matter fluorescence in municipal water recycling schemes: toward a unified PARAFAC model. Environ. Sci. Technol. 45, 2909–2916. https://doi.org/10.1021/es103015e.

Murphy, K.R., Stedmon, C.A., Graeber, D., Bro, R., 2013. Fluorescence spectroscopy and multi-way techniques. PARAFAC. Anal. Methods 5, 6557. https://doi.org/10.1039/c3ay41160e.

Nikolaou, A.D., Lekkas, T.D., 2001. The role of natural organic matter during formation of chlorination by-products: a review. Acta Hydrochim. Hydrobiol. 29, 63. https://doi.org/10.1002/1521-401X(200109)29:2/3<63::AID-AHEH63>3.3.CO;2-3.

Niu, X.Z., Busetti, F., Langsa, M., Croué, J.P., 2016. Roles of singlet oxygen and dissolved organic matter in self-sensitized photo-oxidation of antibiotic norfloxacin under sunlight irradiation. Water Res. 106, 214–222. https://doi.org/10.1016/j.watres.2016.10.002.

Nogueira, R.F.P., Oliveira, M.C., Paterlini, W.C., 2005. Simple and fast spectrophotometric determination of H2O2 in photo-Fenton reactions using metavanadate. Talanta 66, 86–91. https://doi.org/10.1016/j.talanta.2004.10.001.

Oliveira, M., Nunes, M., Barreto Crespo, M.T., Silva, A.F., 2020. The environmental contribution to the dissemination of carbapenem and (fluoro)quinolone resistance genes by discharged and reused wastewater effluents: the role of cellular and extracellular DNA. Water Res. 182. https://doi.org/10.1016/j.watres.2020.116011.

Ormeno-Cano, N., Radjenovic, J., 2022. Electrochemical degradation of antibiotics using flow-through graphene sponge electrodes. J. Hazard. Mater. 431, 128462. https://doi.org/10.1016/j.jhazmat.2022.128462.

Oturan, M.A., Aaron, J.-J., 2014. Advanced oxidation processes in water/wastewater treatment: principles and applications. A review. Crit. Rev. Environ. Sci. Technol. 44, 2577–2641. https://doi.org/10.1080/10643389.2013.829765.

Pignatello, J.J., Oliveros, E., MacKay, A., 2006. Advanced oxidation processes for organic contaminant destruction based on the Fenton reaction and related chemistry. Crit. Rev. Environ. Sci. Technol. 36, 1–84. https://doi.org/10.1080/10643380500326564.

Pouliquen, H., Delépée, R., Larhantec-Verdier, M., Morvan, M.L., Le Bris, H., 2007. Comparative hydrolysis and photolysis of four antibacterial agents (oxytetracycline oxolinic acid, flumequine and florfenicol) in deionised water, freshwater and seawater under abiotic conditions. Aquaculture 262, 23–28. https://doi.org/10.1016/j.aquaculture.2006.10.014.

Prieto-Rodríguez, L., Spasiano, D., Oller, I., Fernández-Calderero, I., Agüera, A., Malato, S., 2013. Solar photo-Fenton optimization for the treatment of MWTP effluents containing emerging contaminants. Catal. Today 209, 188–194. https://doi.org/10.1016/j.cattod.2013.01.002.

Rizzo, L., Manaia, C., Merlin, C., Schwartz, T., Dagot, C., Ploy, M.C., Michael, I., Fatta-Kassinos, D., 2013. Urban wastewater treatment plants as hotspots for antibiotic resistant bacteria and genes spread into the environment: a review. Sci. Total Environ. 447, 345–360. https://doi.org/10.1016/j.scitotenv.2013.01.032.

Rusu, A., Hancu, G., Uivaroşi, V., 2015. Fluoroquinolone pollution of food, water and soil, and bacterial resistance. Environ. Chem. Lett. 13, 21–36. https://doi.org/10.1007/s10311-014-0481-3.

Salmerón, I., Rivas, G., Oller, I., Martínez-Piernas, A., Agüera, A., Malato, S., 2021. Nanofiltration retentate treatment from urban wastewater secondary effluent by solar electrochemical oxidation processes. Sep. Purif. Technol. 254, 117614. https://doi.org/10.1016/j.seppur.2020.117614.

Sciscenko, I., Arques, A., Micó, P., Mora, M., García-Ballesteros, S., 2022. Emerging applications of EEM-PARAFAC for water treatment: a concise review. Chem. Eng. J. Adv. 10, 100286. https://doi.org/10.1016/j.ceja.2022.100286.

Sciscenko, I., Arques, A., Varga, Z., Bouchonnet, S., Monfort, O., Brigante, M., Mailhot, G., 2021a. Significant role of iron on the fate and photodegradation of enrofloxacin. Chemosphere 270, 129791. https://doi.org/10.1016/j.chemosphere.2021.129791.

Sciscenko, I., Garcia-Ballesteros, S., Sabater, C., Castillo, M.A., Escudero-Oñate, C., Oller, I., Arques, A., 2020. Monitoring photolysis and (solar photo)-Fenton of enrofloxacin by a methodology involving EEM-PARAFAC and bioassays: role of pH and water matrix. Sci. Total Environ. 719, 137331. https://doi.org/10.1016/j.scitotenv.2020.137331.

Sciscenko, I., Thị Mỹ Hằng, H., Escudero-Oñate, C., Oller, I., Arques, A., 2021b. Fluorescence spectroscopy and chemometrics: a simple and easy way for the monitoring of fluoroquinolone mixture degradation. ACS Omega 6, 4663–4671. https://doi.org/10.1021/acsomega.0c05370.

Serna-galvis, E.A., Martínez-mena, Y.L., Porras, J., Ávila-torres, Y., Silva-agredo, J., Torres-palma, R.A., 2021. Understanding the role of complexation of fluoroquinolone and β-lactam antibiotics with iron (Iii) on the photodegradation under solar light and uvc light. Water (Switzerland) 13. https://doi.org/10.3390/w13182603.

Sgroi, M., Roccaro, P., Korshin, G.V., Greco, V., Sciuto, S., Anumol, T., Snyder, S.A., Vagliasindi, F.G.A., 2017. Use of fluorescence EEM to monitor the removal of emerging contaminants in full scale wastewater treatment. J. Hazard. Mater. 323, 367–376. https://doi.org/10.1016/j.jhazmat.2016.05.035.

Shutova, Y., Baker, A., Bridgeman, J., Henderson, R.K., 2014. Spectroscopic characterisation of dissolved organic matter changes in drinking water treatment: from PARAFAC analysis to online monitoring wavelengths. Water Res. 54, 159–169. https://doi.org/10.1016/j.watres.2014.01.053.

Snowberger, S., Adejumo, H., He, K., Mangalgiri, K.P., Hopanna, M., Soares, A.D., Blaney, L., 2016. Direct photolysis of fluoroquinolone antibiotics at 253.7 nm: specific reaction kinetics and formation of equally potent fluoroquinolone antibiotics. Environ. Sci. Technol. 50, 9533–9542. https://doi.org/10.1021/acs.est.6b01794.

Soler, J., Santos-Juanes, L., Miró, P., Vicente, R., Arques, A., Amat, A.M., 2011. Effect of organic species on the solar detoxification of water polluted with pesticides. J. Hazard. Mater. 188, 181–187. https://doi.org/10.1016/j.jhazmat.2011.01.089.

Turel, I., 2002. The interactions of metal ions with quinolone antibacterial agents. Coord. Chem. Rev. 232, 27–47. https://doi.org/10.1016/S0010-8545(02)00027-9.

Urbaniak, B., Kokot, Z.J., 2009. Analysis of the factors that significantly influence the stability of fluoroquinolone-metal complexes. Anal. Chim. Acta 647, 54–59. https://doi.org/10.1016/j.aca.2009.05.039.

Van Doorslaer, X., Dewulf, J., Van Langenhove, H., Demeestere, K., 2014. Fluoroquinolone antibiotics: an emerging class of environmental micropollutants. Sci. Total Environ. 500–501, 250–269. https://doi.org/10.1016/j.scitotenv.2014.08.075.

Von Gunten, U., 2003. Ozonation of drinking water: part II. Disinfection and by-product formation in presence of bromide, iodide or chlorine. Water Res. 37, 1469–1487. https://doi.org/10.1016/S0043-1354(02)00458-X.

Xu, R., Cao, J., Feng, G., Luo, J., Feng, Q., Ni, B., Fang, F., 2021. Fast identification of fluorescent components in three-dimensional excitation-emission matrix fluorescence spectra via deep learning. Chem. Eng. J. 132893. https://doi.org/10.1016/j.cej.2021.132893.

Yang, L., Hur, J., Zhuang, W., 2015. Occurrence and behaviors of fluorescence EEM-PARAFAC components in drinking water and wastewater treatment systems and their applications: a review. Environ. Sci. Pollut. Res. 22, 6500–6510. https://doi.org/10.1007/s11356-015-4214-3.

Zhang, H., Huang, C.H., 2005. Oxidative transformation of fluoroquinolone antibacterial agents and structurally related amines by manganese oxide. Environ. Sci. Technol. 39, 4474–4483. https://doi.org/10.1021/es048166d.

Zhang, Z., Xie, X., Yu, Z., Cheng, H., 2019. Influence of chemical speciation on photochemical transformation of three fluoroquinolones (FQs) in water: kinetics, mechanism, and toxicity of photolysis products. Water Res. 148, 19–29. https://doi.org/10.1016/j.watres.2018.10.027.